Zhang et al. J Infrastruct Preserv Resil (2023) 4:13
https://doi.org/10.1186/s43065-023-00074-9

Journal of Infrastructure Preservation and Resilience

RESEARCH

Open Access

Dynamic responses of a train-track-bridge coupled system under earthquakes

Xuebing Zhang[1], Han Wu[1], Han Zhao[2*] and Ping Xiang[2*]

Abstract

The probability of a train running over a bridge when an earthquake occurs is increasing with the total mileage of China's high-speed railway network expanding. To study this issue, a three-dimensional train-track-bridge dynamic interaction system subjected to seismic excitations is established based on commercial mathematical software. Besides, a set of motion equations of the system are derived according to the multibody dynamics, the finite element method theory and the bridge seismic theory. Moreover, in order to study the dynamic response of high-speed railway bridges under earthquake, a series of experiments are conducted on a scaled high-speed railway simple supported bridge model with a ballastless track slab excited by shaking table tests. Meanwhile, the strain of rails, track slabs, base plates and girder in various working conditions are measured by quasi-distributed optical fiber sensing stuck in bridge members. At last, the dynamic response of each structure member is demonstrated in the time and frequency domains. Furthermore, the seismic isolation performance of bridge members, such as fasteners, cement asphalt (CA) mortar layer and so on, is explained in details.

Keywords Train-bridge dynamic interaction, Model experiments, Seismic isolation performance, Frequency analysis, Earthquake

Introduction

In order to meet the transport demand, high-speed railways (HSRs) have been constructed rapidly in China [20, 21]. By the end of 2021, the total mileage of China's HSR has exceeded forty thousand kilometers. The bridge accounts for a high proportion of the whole HSR lines, out of consideration for the train running stability, land occupation, environmental protection, foundation reliability, etc. [15, 22, 30]. With the increasing operation mileage, the scope of HSR lines has expanded to earthquake-prone areas. Therefore, it is necessary to study the seismic performance of the bridge structure when the train-bridge system encounters an earthquake to ensure the train running safety.

Many scholars have conducted massive research on the dynamic response of trains and bridges in a train-bridge system under earthquake. Xia et al. established a dynamic model for train bridge interaction based on the wheel-rail interaction theory, considering different seismic wave inputs [32]. Du et al. proposed a finite element method (FEM) framework for analyzing the dynamic behavior of a train-bridge system under non-uniform seismic excitation [7]. Li et al. established a simply supported bridge model with a China railway track system (CRTS) II ballastless track slab and studied the influence of isolation bearing's equivalent radius on bridge response under random earthquake excitation [23]. Zhang et al. calculated the random vibration of a train-bridge system under a multi-point earthquake using the pseudo-excitation method [42]. Ling et al. studied the earthquake's impact on the dynamic

*Correspondence:
Han Zhao
hanzhao@csu.edu.cn
Ping Xiang
pxiang2-c@my.cityu.edu.hk
[1] College of Civil Engineering and Mechanics, Xiangtan University, Xiangtan, Hunan 411105, China
[2] School of Civil Engineering, Central South University, Changsha 410075, Hunan, China

behavior of trains and tracks and proposed safety criteria for train running safety [24]. Jiang et al. used a new point estimation method to calculate the random dynamic response of a three-dimensional train-bridge system [16]. Zhang et al. proposed an efficient method to calculate the seismic response of HSR, considering the influence of track longitudinal constraints on bridges [41]. Liu et al. calculated the bridge response limit according to the derailment coefficient [25].

In order to prove the validity of numerical simulation results, many train-bridge experiments are introduced in detail. Toyooka et al. compared the dynamic behavior of the track structure under the shaking table test with the calculation results of a simulation model [31]. They calculated and analyzed the influence of the track structure on the bridge response. Nishimura et al. compared the simulation calculation and experimental results of the displacement time history of trains and tracks to verify the performance of anti-derailment guardrails [27]. Guo et al. proposed a superposition algorithm to calculate the bridge damage caused by an earthquake and the influence on the train running safety, and the accuracy of the numerical value was verified by shaking table experiments [12]. Yu et al. summarized the track irregularity deformation pattern under earthquake by calculating the simple supported bridge model verified by experiments [39]. In order to study the impact of a train on a bridge vibration, Chen et al. analyzed the seismic response of different piers under different speeds [4]. Yu et al. studied the influence of train and ground motion on the deformation of the beam, bearing and pier based on the simulation model verified by shaking table experiments [37, 38]. Gao et al. considered the incident angle of seismic waves. They calculated and analyzed the seismic impact of the train speed on the bridge structure, and the results showed that the dynamic bridge response reached the maximum within a specific range of train speed [9].

The existing train-bridge coupling related literature mainly studies the seismic response of substructures such as beams, bearings and piers. However, research on the seismic dynamic behavior of track structures is rare. The rail directly contacts the train, and the deformation of the track structure directly affects the train running safety. In addition, the impact of the train operation on the bridge also cannot be ignored. Therefore, the seismic response of the track structure is critical to the dynamic response of the train and bridge.

In this paper, a series of experiments are performed based on a train running test system (TRTS). Meanwhile, the TRTS consists of a scaled train model, scaled CRTS type II slab ballastless tracks, a scaled 11-span simply supported bridge and four shaking tables. In the experiments, the strain of the rails, track slabs, base plates and beam is measured and analyzed. Furthermore, a train-bridge coupled (TBC) system is established according to the prototype of the TRTS, based on the bridge seismic theory and the finite element theory. After verifying the TBC system, the three-dimensional dynamic responses of the rails, track slabs, base plates and beam under earthquake are discussed and analyzed.

Simulation model

A dynamic model under uniform seismic excitations is set up by considering the seismic force boundary of the subgrade and bridge. The model consists of a series of train models with 38 degrees of freedom (DOFs) individually, a ballastless track model with three layers of elastic point support and a bridge model [11] (Fig. 1). Secondly, the trace line method is applied to solve the spatial geometric contact of the wheel-rail. Besides, the Hertz contact theory [18] is adopted to calculate the normal force,

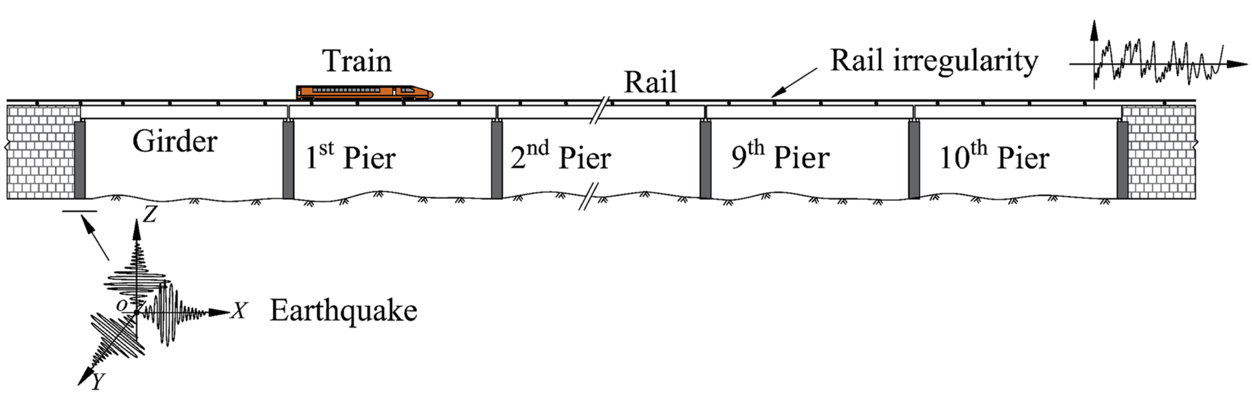

Fig. 1 Schematic diagram of the TBC model

and the Kalker linear rolling contact theory [19] is used to formulate the creep forces.

Model of train

HSR train is a three-dimensional vibration system with an elastic suspension device. It can be assumed that the car-body, bogies and wheel-sets are rigid bodies to improve numerical efficiency, except for the fatigue analysis or high-frequency vibration analysis of the train. Besides, the coupler and suspension system of the train are simulated with a three-dimensional linear spring-damper. And secondly, the train is composed of four-axle motor cars and trailers in a certain formation. Each vehicle has one car-body with six DOFs, two bogies with six DOFs each and four wheel-sets with five DOFs each. The schematic diagram of the vehicle is shown in Fig. 2. Table 1 lists the symbols of basic motions, such as longitudinal, lateral, vertical, roll, pitch and yaw. Wherein the symbols of train vibration DOFs can be expressed as:

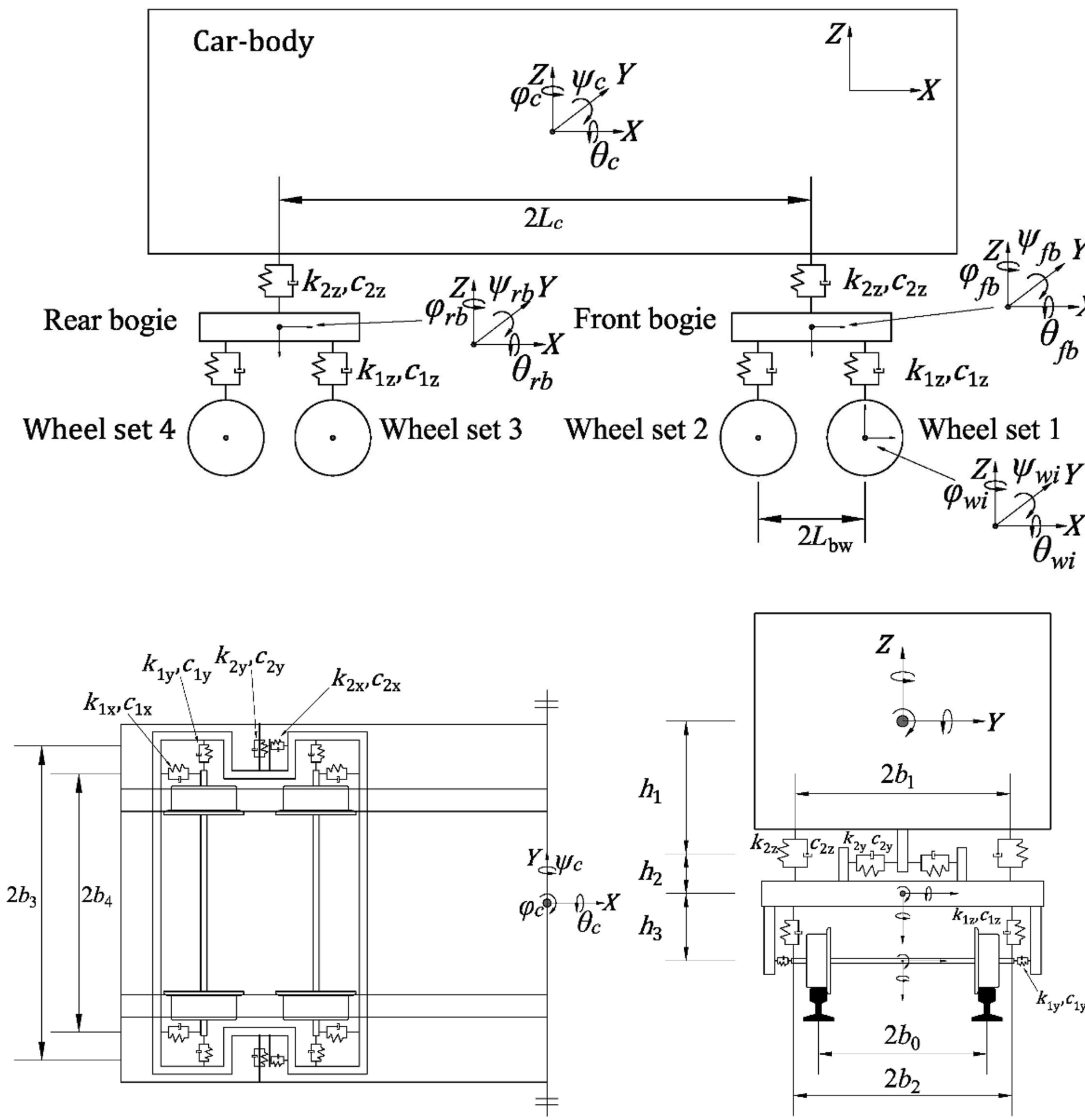

Fig. 2 Schematic diagram of train model

Table 1 DOFs of the train [44]

Vehicle components	DOFs					
	Longitudinal	Lateral	Vertical	Roll	Pitch	Yaw
Car-body	x_c	y_c	z_c	θ_c	ψ_c	φ_c
Front bogie	x_{fb}	y_{fb}	z_{fb}	θ_{fb}	ψ_{fb}	φ_{fb}
Rear bogie	x_{rb}	y_{rb}	z_{rb}	θ_{rb}	ψ_{rb}	φ_{rb}
Wheel-sets, $i=1\sim4$	x_{wi}	y_{wi}	z_{wi}	θ_{wi}	–	φ_{wi}

$$\mathbf{X}_v = \left\{ \left(\mathbf{X}_{c,v}, \mathbf{X}_{fb,v}, \mathbf{X}_{rb,v}, \mathbf{X}_{w1,v}, \mathbf{X}_{w2,v}, \mathbf{X}_{w3,v}, \mathbf{X}_{w4,v} \right)_v \middle| 1 \le v \le n_v \quad v, n_v \in Z \right\} \tag{1}$$

With

$$\begin{cases} \mathbf{X}_{i,v} = \left(x_{i,v}, y_{i,v}, z_{i,v}, \theta_{i,v}, \psi_{i,v}, \varphi_{i,v} \right), & i \subseteq (c, fb, rb) \\ \mathbf{X}_{j,v} = \left(x_{j,v}, y_{j,v}, z_{j,v}, \theta_{j,v}, \varphi_{j,v} \right), & j \subseteq (w1, w2, w3, w4) \end{cases} \tag{2}$$

Where subscript c, fb and rb denote car-body, front bogie and rear bogie, respectively. Subscript wi means the i^{th} wheel-set and subscript v means the v^{th} vehicle, which is n_v in total.

The train's mass, stiffness and damping matrices can be referred to Ref. [43].

Model of track slab and bridge

As reference in Fig. 3, eleven-span prestressed HSR two-way simply supported box-girder with concrete piers (bridge) and CRTS type II slab ballastless track are adopted in this paper, which is modelled based on the FEM [10, 35]. The bridge and slab ballastless track are modelled based on the FEM [14]. The element parameters of bridge components are listed in Table 2. Besides, the earthquake excitations are directly forced at supporting points at the bottom of the bridge pier and their effect on the bridge is reflected by the influence matrix [1].

The damping dissipation model is so complicated that a specific mathematical formula cannot describe it. Therefore, in order to avoid excessive calculation, some simplified damping dissipation models have been used in the TBC system, including the Rayleigh damping model, the Caughey damping model and so on. Liu et al. compared the influence of the Rayleigh damping model and Caughey damping model on the stochastic analysis, and concluded that the variation of the damping ratio of the two models has little influence on the TBC stochastic analysis results. Moreover, they indicated that the Rayleigh damping model has enough accuracy to show the dissipation of the system [26]. So, the Rayleigh damping model is adopted in this paper, which can be expressed as follow:

$$\mathbf{C}_{bb} = \frac{2\omega_i\omega_j\zeta_b}{\omega_i + \omega_j}\mathbf{M}_{bb} + \frac{2\zeta_b}{\omega_i + \omega_j}\mathbf{K}_{bb} \tag{3}$$

Where ω_i means the first-order natural frequency of the bridge, which is 10.0752 rad/s; ω_j means the second-order natural frequency of the bridge, which is 11.0096 rad/s; ζ_b represents the damping ratio of the bridge, which is 0.03 in this research [17, 36].

The interactive stiffness matrices and damping matrices of rail and bridge satisfied:

$$\mathbf{K}_{br} = \mathbf{K}_{br}^{\mathbf{T}}, \mathbf{C}_{br} = \mathbf{C}_{br}^{\mathbf{T}} \tag{4}$$

Wheel-rail interaction

Wheel-rail contact geometry

The wheel-rail relationship is the bond of train and track and keeps updating with each time step of the system motion equation. Besides, the wheel-rail contact model is established on the assumption that the wheels are rigidly in contact with the rails, and there are no compressions between them [34]. Consequently, the spatial geometric relationship of wheel-rail contact can be calculated, and the schematic diagram is shown in Fig. 4.

The coordinate of the wheel-rail contact point in the absolute coordinate system can be deduced as

$$\begin{cases} x_{C^R} = x_B + l_x R_w \tan\delta_R \\ y_{C^R} = y_B - \frac{R_w}{1-l_x^2}\left(l_x^2 l_y \tan\delta_R + l_z\sqrt{1 - l_x^2\left(1 + \tan^2\delta_R\right)} \right) \\ z_{C^R} = z_B - \frac{R_w}{1-l_x^2}\left(l_x^2 l_y \tan\delta_R - l_y\sqrt{1 - l_x^2\left(1 + \tan^2\delta_R\right)} \right) \end{cases} \tag{5}$$

With

$$\begin{cases} x_B = d_w l_x \\ y_B = d_w l_y + Y_w \\ z_B = d_w l_z \end{cases} \tag{6}$$

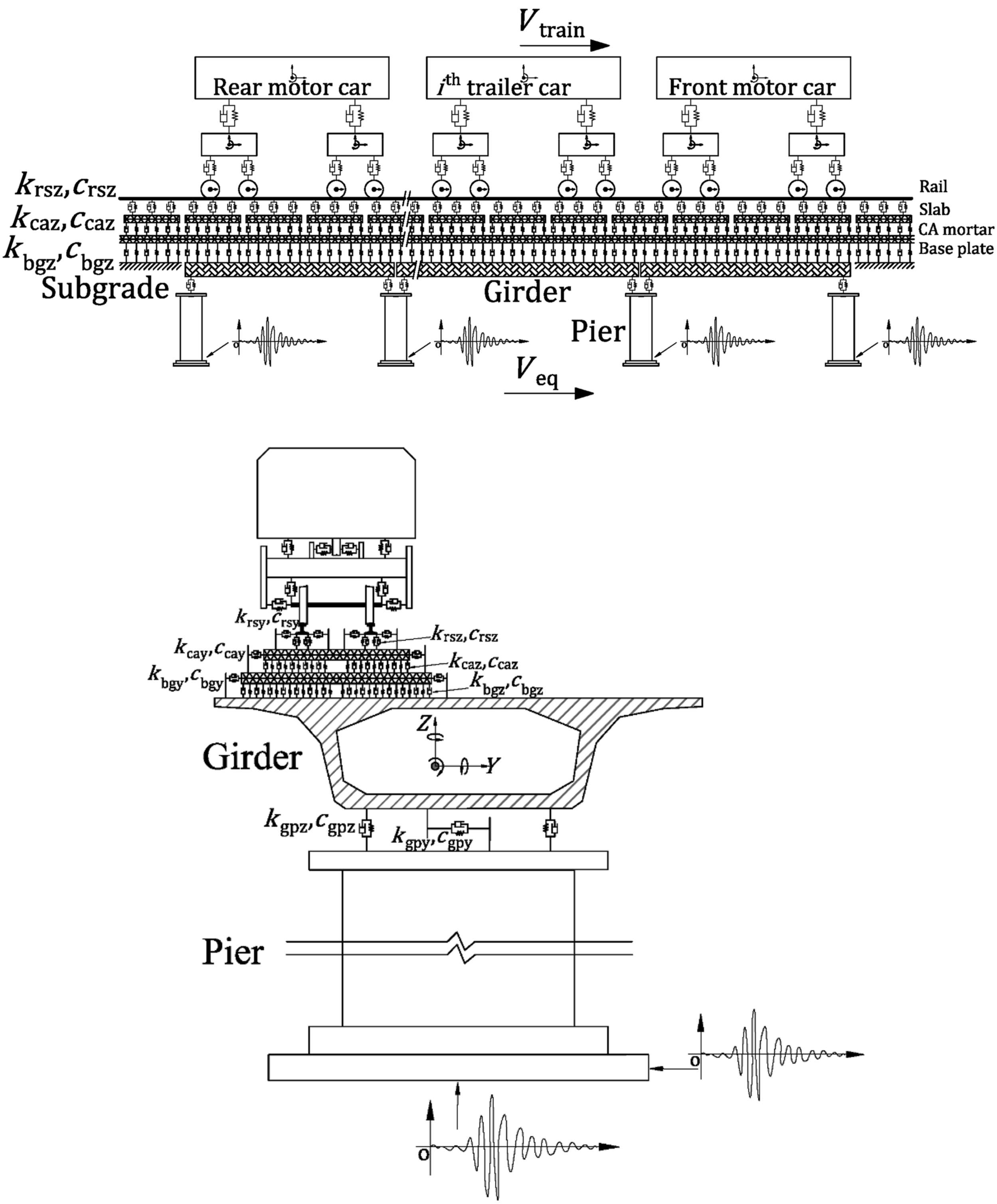

Fig. 3 Schematic diagram of track slab and bridge model

Table 2 Element parameters of the bridge model

FEM model	Element type	Element length (m)
Rail	Beam	0.615
Track slab	Plate	0.615
Base plate	Plate	0.615
Girder	Beam	0.615
Pier	Beam	1

$$\begin{cases} l_x = -\sin\varphi_w \cos\psi_w \\ l_y = \cos\varphi_w \cos\psi_w \\ l_z = \sin\varphi_w \end{cases} \tag{7}$$

Where δ_R means the contact angle of the right wheel tread. R_w denotes the rolling radius of wheel. l_x, l_y, l_z are the direction cosines of the x-axis, y-axis, z-axis, respectively. x_B, y_B, z_B represent the coordinates of the wheel rolling circle center. d_w means the abscissa of wheel rolling circle in the wheel coordinate. The wheel-rail contact trace line can be formed by changing d_w in the wheel coordinate.

Wheel-rail normal force

According to the wheel-rail rigidly contact assumption, the wheel-rail normal force can be solved by Hertz nonlinear elastic contact theory:

$$N(t) = \left[\frac{1}{G}\delta Z(t)\right]^{3/2} \tag{8}$$

Where $N(t)$ means the time-varying function of wheel-rail normal force; $G=3.86R_w^{-0.115}\times10^{-8}(m/N)^{2/3}$ represents the wheel-rail contact constant; R_w is the radius of the wheel; and $\delta Z(t)$ is the normal compression displacement between wheel and rail.

A simplified method proposed by Zhai et al. [40] is adopted to deduce the wheel-rail normal compression displacement $\delta Z(t)$. Firstly, the j^{th} wheel-sets vertical relative distance between the wheel and rail at time t needs to be obtained according to Eq. (9).

$$\begin{cases} \delta Z_{\mathrm{Lj}} = Z_{\mathrm{wj}}(t) - \left(\Delta Z_{\mathrm{Lwjt}} - \Delta Z_{\mathrm{Lwj0}}\right) \\ \delta Z_{\mathrm{Rj}} = Z_{\mathrm{wj}}(t) - \left(\Delta Z_{\mathrm{Rwjt}} - \Delta Z_{\mathrm{Rwj0}}\right) \end{cases} \tag{9}$$

Where $Z_{wj}(t)$ means the vertical displacement of the centroid of the j^{th} wheel-set; ΔZ_{Lwjt} and ΔZ_{Rwjt} are the left and right j^{th} wheel-sets minimum vertical distance between wheel and rail at time t, respectively; ΔZ_{Lwj0} and ΔZ_{Rwj0} are the left and right j^{th} wheel-sets minimum vertical distance between wheel and rail at zero time, respectively, which are equal due to the symmetry of wheel-sets, that is $\Delta Z_{Lwj0}=\Delta Z_{Rwj0}=\Delta Z_{wj0}$.

Secondly, the wheel-rail normal compression can be deduced from the wheel-rail vertical relative displacement based on the spatial geometric relationship [29]. Therefore, the normal compression displacement of left and right wheel-rail contact points satisfy:

$$\begin{cases} \delta Z_{\mathrm{Lcj}} = \frac{\delta Z_{\mathrm{L}}}{\cos(\delta_{\mathrm{L}}+\phi_{\mathrm{W}})} \\ \delta Z_{\mathrm{Rcj}} = \frac{\delta Z_{\mathrm{Rj}}}{\cos(\delta_{\mathrm{R}}-\phi_{\mathrm{w}})} \end{cases} \tag{10}$$

In particular, the wheel-rail normal force $N(t)=0$, when the normal compression displacement between wheel

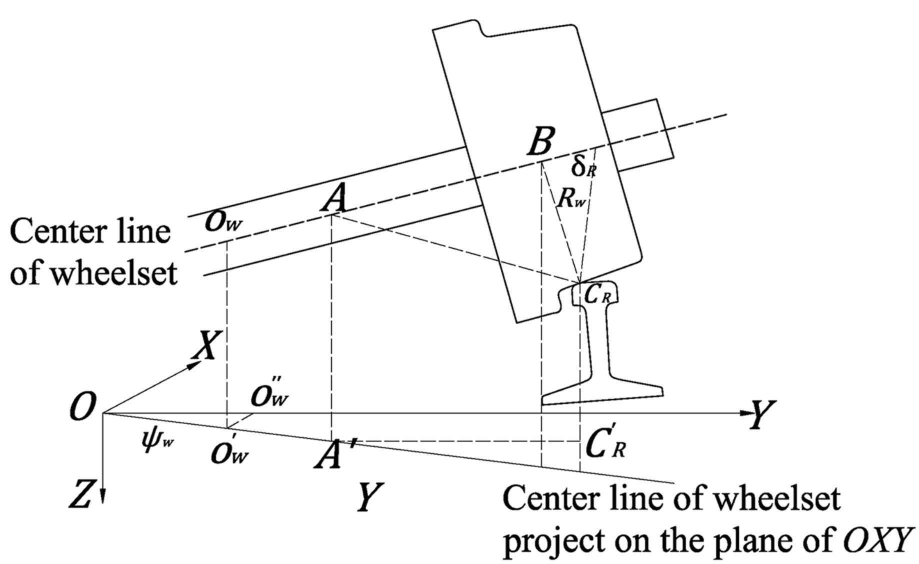

Fig. 4 Schematic diagram of spatial wheel-rail contact

and rail $\delta Z(t) < 0$, and the wheel-rai are detached at the moment.

Wheel-rail creep force

The wheel-rail creep force is formulated according to Kalker linear rolling contact theory [19]. The longitudinal wheel-rail creep force F_x, lateral creep force F_y, and rotating creep moment M_z within the linear range can be expressed as:

$$\begin{cases} F_x = -f_{11}\xi_x \\ F_y = -f_{22}\xi_y - f_{23}\xi_\varphi \\ M_z = f_{23}\xi_y - f_{33}\xi_\varphi \end{cases} \tag{11}$$

Where ξ_x, ξ_y, and ξ_φ are the longitudinal creep rate, lateral creep rate and rotating creep rate, respectively. Eq. (11) is suitable for both sides of wheel. f_{ij} represents the creep coefficient, which can be accurately calculated according to Ref. [19]:

$$\begin{cases} f_{11} = 0.5E_r(1+\nu_r)^{-1}(ab)C_{11} \\ f_{22} = 0.5E_r(1+\nu_r)^{-1}(ab)C_{22} \\ f_{23} = 0.5E_r(1+\nu_r)^{-1}(ab)^{3/2}C_{23} \\ f_{33} = 0.5E_r(1+\nu_r)^{-1}(ab)^{2}C_{33} \end{cases} \tag{12}$$

Where E_r and ν_r are the elastic modulus and Poisson's ratio of rail, respectively. C_{ij} is a function of ratio of the long and short axis of the ellipse a/b. a, b can be obtained by inducting parameters a_e, b_e, and ρ,:

$$\begin{cases} a = a_e(NR_w)^{1/3} \\ b = b_e(NR_w)^{1/3} \\ ab = a_e b_e (NR_w)^{2/3} \end{cases} \tag{13}$$

Where N means the normal force of the wheel-rail contact point. a_e and b_e can be expressed as:

$$\begin{cases} a_\mathrm{e} = 0.1506\mathrm{m}\left(\frac{\rho}{\mathrm{R_w}}\right)^{1/3} \times 10^{-3} & \rho/R_w \le 2 \\ b_\mathrm{e} = 0.1506n\left(\frac{\rho}{R_w}\right)^{1/3} \times 10^{-3} & \\ a_\mathrm{e} = 0.1506n\left(\frac{\rho}{R_w}\right)^{1/3} \times 10^{-3} & \rho/R_w > 2 \\ \mathrm{b_e} = 0.1506m\left(\frac{\rho}{R_w}\right)^{1/3} \times 10^{-3} & \end{cases} \tag{14}$$

Where ρ satisfies $\frac{1}{\rho} = \frac{1}{4}\left[\frac{1}{R_n} + \left(\frac{1}{r_m} + \frac{1}{r_r}\right)\right]$. r_w means the cross-section profile radius of the wheel tread. r_r is the cross-section profile radius of rail head. m and n are coefficients related to the angle β, where $\beta = \arccos\left(\frac{\rho}{4}\left|\frac{1}{R_w} - \frac{1}{r_w} - \frac{1}{r_r}\right|\right)$. More details can be found in Ref. [19].

Motion equation under uniform earthquake

The earthquake loads are treated as external excitations in the TBC system, and the acceleration input mode is adopted. It is assumed that the bridge piers are connected to the ground through the supporting nodes. Wherein the dynamic equation of the system is partitioned as supporting nodes block matrix (supporting nodes) and structures block matrix (structure nodes). And the dynamic equation can be expressed as follows [44].

$$\begin{bmatrix} \mathbf{M}_{ss} & \mathbf{M}_{sb} \\ \mathbf{M}_{bs} & \mathbf{M}_{bb} \end{bmatrix}\begin{Bmatrix} X_s'' \\ X_b'' \end{Bmatrix} + \begin{bmatrix} \mathbf{C}_{ss} & \mathbf{C}_{sb} \\ \mathbf{C}_{bs} & \mathbf{C}_{bb} \end{bmatrix}\begin{Bmatrix} X_s' \\ X_b' \end{Bmatrix} + \begin{bmatrix} \mathbf{K}_{ss} & \mathbf{K}_{sb} \\ \mathbf{K}_{bs} & \mathbf{K}_{bb} \end{bmatrix}\begin{Bmatrix} X_s \\ X_b \end{Bmatrix} = \begin{Bmatrix} 0 \\ f_b \end{Bmatrix} \tag{15}$$

Where $\{X_b\}$ means the enforced displacements of the supporting nodes; $\{X_s\}$ represent the displacements of structure nodes; $\{\mathbf{M}_{ss}\}$, $\{\mathbf{C}_{ss}\}$ and $\{\mathbf{K}_{ss}\}$ are mass matrix, damping matrix and stiffness matrix of the structure nodes, respectively; $\{\mathbf{M}_{bb}\}$, $\{\mathbf{C}_{bb}\}$ and $\{\mathbf{K}_{bb}\}$ are mass matrix, damping matrix and stiffness matrix of the supporting nodes, respectively; $\{\mathbf{M}_{sb}\}$, $\{\mathbf{M}_{bs}\}$, $\{\mathbf{C}_{sb}\}$, $\{\mathbf{C}_{bs}\}$, $\{\mathbf{K}_{sb}\}$ and $\{\mathbf{K}_{bs}\}$ denote the coupling mass matrices, the coupling damping matrices and the coupling stiffness matrices of the supporting nodes and the structure nodes; $\{f_b\}$ is the force of the supporting nodes subject to the ground.

The first row of Eq. (15) is expanded based on the lumped mass assumption [28], and it can be calculated that:

$$[\mathbf{M}_{ss}]\{X_s''\} + [\mathbf{C}_{ss}]\{X_s'\} + [\mathbf{K}_{ss}]\{X_s\} = -[\mathbf{C}_{sb}]\{X_b'\} - [\mathbf{K}_{sb}]\{X_b\} \tag{16}$$

Where $\{X_s\}$ is decomposed into pseudo-static displacement $\{Y_s\}$ and dynamic displacement $\{Y_r\}$, namely:

$$\{X_s\} = \{Y_s\} + \{Y_r\} \tag{17}$$

The pseudo-static displacement $\{Y_s\}$ satisfies static equilibrium equation (set all dynamic displacement to zero), hence $\{Y_s\}$ can be deduced as follows.

$$\{Y_s\} = [\mathbf{R}]\{X_b\} \tag{18}$$

Thus, the pseudo-static velocity and acceleration can be obtained based on Eq. (18).

$$\{Y_s'\} = [\mathbf{R}]\{X_b'\} \tag{19}$$

$$\{Y_s''\} = [\mathbf{R}]\{X_b''\} \tag{20}$$

Where $[\mathbf{R}] = -[\mathbf{K}_{ss}]^{-1}[\mathbf{K}_{sb}]$ means the influence matrix.

Especially the damping force is considered to be proportional to the dynamic velocity $\{Y_r^{'}\}$, so Eq. (16) can be transformed into:

$$[\mathbf{M}_{ss}]\{Y_r''\} + [\mathbf{C}_{ss}]\{Y_r'\} + [\mathbf{K}_{ss}]\{Y_r\} = -[\mathbf{M}_{ss}]\{Y_s''\} - [\mathbf{C}_{sb}]\{X_b'\} - [\mathrm{K}_{ss}]\{Y_s'\} - [\mathrm{K}_{sb}]\{X_b\} \tag{21}$$

Then, According to Eqs. (18) and (20) and ignoring the damping force of the supporting nodes $[\mathrm{C_{sb}}]\{\mathrm{X_b'}\}$, Eq. (21) can be recast as:

$$[\mathbf{M}_{ss}]\{Y_r''\} + [\mathbf{C}_{ss}]\{Y_r'\} + [\mathbf{K}_{ss}]\{Y_r\} = -[\mathbf{M}_{ss}][\mathbf{R}]\{X_b''\} \tag{22}$$

Considering $\{X_b''\} = \left\{X_g''\right\}$ and the seismic ground motion, hence Eq. (22) can be written as:

$$[\mathbf{M}_{ss}]\{Y_r''\} + [\mathbf{C}_{ss}]\{Y_r'\} + [\mathbf{K}_{ss}]\{Y_r\} = -[\mathbf{M}_{ss}][\mathbf{R}]\left\{X_g''\right\} \tag{23}$$

Furthermore, the energy variational method is introduced to calculate the train subsystem and track-bridge subsystem. Moreover, a two-step unconditionally stable explicit displacement method was employed to solve the dynamic response of the system [3].

Rail irregularity

The track irregularities appreciably affect the lateral vibration and the short-wavelength irregularities will activate a high-frequency vibration in the vertical direction. Thus, the influence of primary rail irregularity on dynamic train response should be considered. The rail irregularity in the TBC system is generated by the harmonic synthesis method combined with German low-disturbance power spectral density (PSD) [13]. which can be expressed as.

the rail elevation irregularity:

$$S_v(\Omega) = \frac{A_v \Omega_c^2}{\left(\Omega^2 + \Omega_r^2\right)\left(\Omega^2 + \Omega_c^2\right)} \tag{24}$$

the rail alignment irregularity:

$$S_a(\Omega) = \frac{A_a \Omega_c^2}{\left(\Omega^2 + \Omega_c^2\right)\left(\Omega^2 + \Omega_c^2\right)} \tag{25}$$

the rail cross level irregularity:

$$S_c(\Omega) = \frac{A_v b^{-2} \Omega_c^2 \Omega}{\left(\Omega^2 + \Omega_r^2\right)\left(\Omega^2 + \Omega_c^2\right)\left(\Omega^2 + \Omega_s^2\right)} \tag{26}$$

the rail gauge irregularity:

$$S_g(\Omega) = \frac{A_g \Omega_c^2 \Omega^2}{\left(\Omega^2 + \Omega_r^2\right)\left(\Omega^2 + \Omega_c^2\right)\left(\Omega^2 + \Omega_s^2\right)} \tag{27}$$

Where S_v, S_a, and S_g are the irregularity PSD function of vertical rail profile, rail alignment and gauge distance, respectively [$\mathrm{m^2/(rad/m)}$]; S_c is the PSD function of rail cross-level irregularity [$1/(\mathrm{rad/m})$]; A_v, A_a, and A_g represent the roughness coefficients; Ω_c, Ω_r and Ω_s mean the truncation frequency; b denotes the half distance between two sides of the rail. The detailed parameters of the irregularity PSD function are shown in Table 3.

Experimental design

Experiment model

In order to verify the accuracy of the established TBC model, the TRTS experiments are performed. The TRTS is shown in Fig. 5, and the experiment results are compared with the simulation results.

The TRTS consists of four shaking tables, a scaled two-way simply supported bridge model, a scaled CRH2 model train, an acceleration section, a deceleration section and a transition section. The bridge model has a scale of 1:10 compared with the prototype and eleven spans with a span of 3.25 m. Table 4 lists the similarity coefficient of the TRTS.

The scaled bridge model and fasteners were made of steel for easy installation. Besides, the rails, slab tracks, base plates, beam and piers in the TRTS were fabricated based on the equivalent bending stiffness of the prototype. The shear reinforcement, shear slots and block in the TRTS were fabricated based on equivalent displacement and force. Furthermore, the sliding layer material is the same as the prototype and the CA mortar layer is replaced by polyurethane. The four shaking tables are all 6-DOF mobile tables, and the maximum bearing capacity of each shaking table is 30 tons.

The experiment process is as follows: the model train is accelerated to the target speed by the acceleration board before entering the transition section. When the train enters the scaled bridge model, the transition device is immediately disconnected, and the four shaking tables vibrate according to the input ground motion. After the model train enters the deceleration

Table 3 Parameters of German low-disturbance PSD of rail irregularity [33]

Ω_c/ (rad/m)	Ω_r/ (rad/m)	Ω_s/ (rad/m)	A_a/ ($\mathrm{m^2}$·rad/m)	A_v/ ($\mathrm{m^2}$·rad/m)	A_g/ ($\mathrm{m^2}$·rad/m)
0.8246	0.0206	0.438	2.119×10^{-7}	4.032×10^{-7}	5.32×10^{-7}

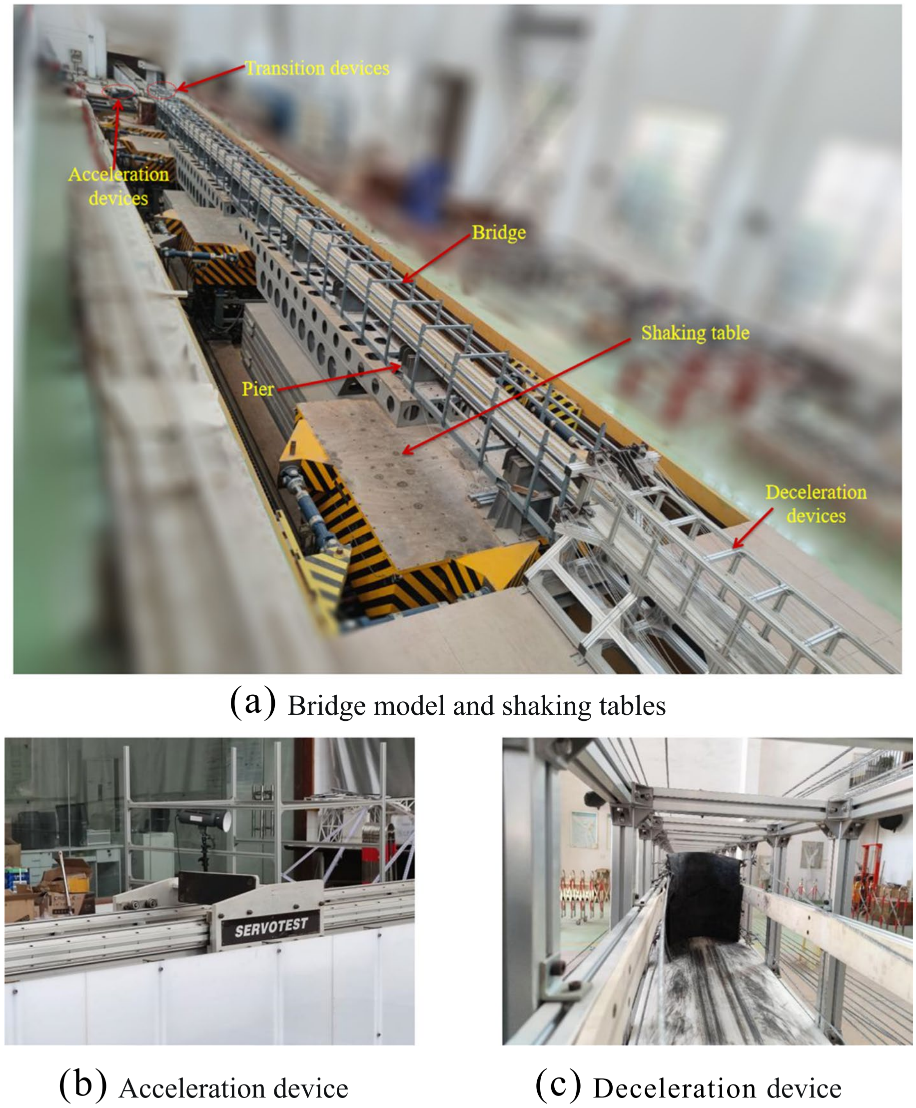

Fig. 5 The train running test system

Table 4 The similarity coefficients of the TRTS (partial data refer to [37])

Similarity coefficient	Symbol	Scaling equation	Value	Description
Acceleration	S_A	$S_A = S_A$	1/1	Basic parameter
Length	S_L	$S_L = S_L$	1/10	Basic parameter
Stress	S_σ	$S_\sigma = S_\sigma$	1/2	Basic parameter
Elastic modulus	S_E	$S_E = S_\sigma$	1/2	
Force	S_F	$S_F = S_\sigma \cdot S_L^2$	1/200	
Stiffness	S_S	$S_S = S_\sigma \cdot S_L$	1/20	
Time	S_T	$S_T = (S_l \cdot S_a)^{0.5}$	0.316	
Speed	S_v	$S_v = S_L / S_T$	0.316	

section, the steel cage captures and slows down the train until it stops. In the whole process of the train running on the bridge, the train speed is considered to be constant.

Measuring equipment

In this experiment, a 3.6 m long optical fiber with seven grating points engraved on the steel rail, track slab, base plate and beam of the 7th span of the bridge is laid, respectively, as shown in Fig. 6. Meanwhile, the grating points with an interval of 0.35 m are used to collect the strain of the pertinent bridge members under earthquake.

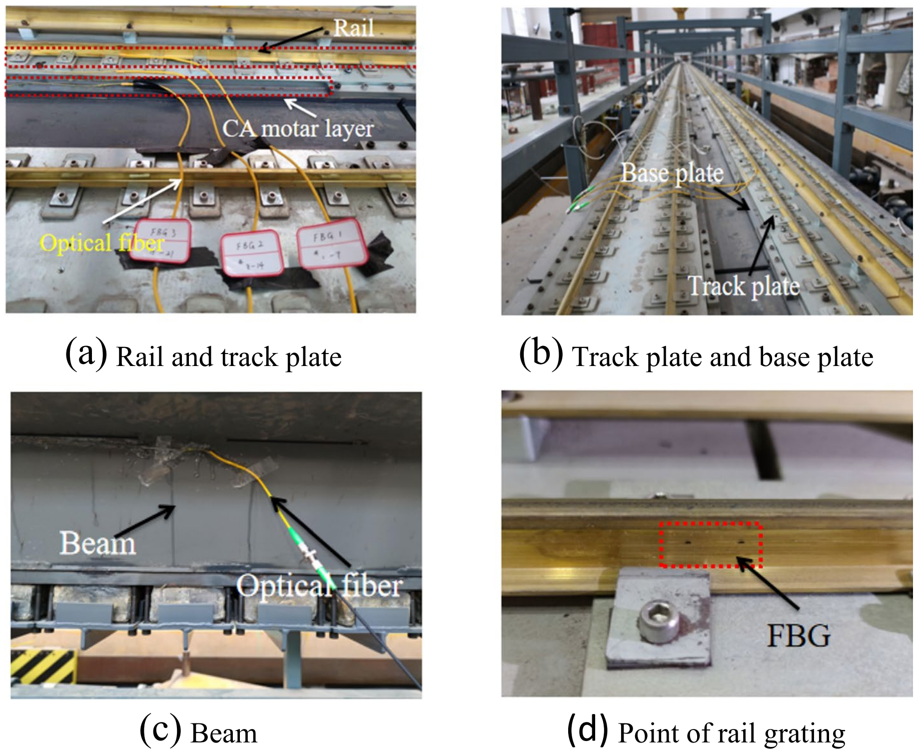

Fig. 6 FBG configuration diagram

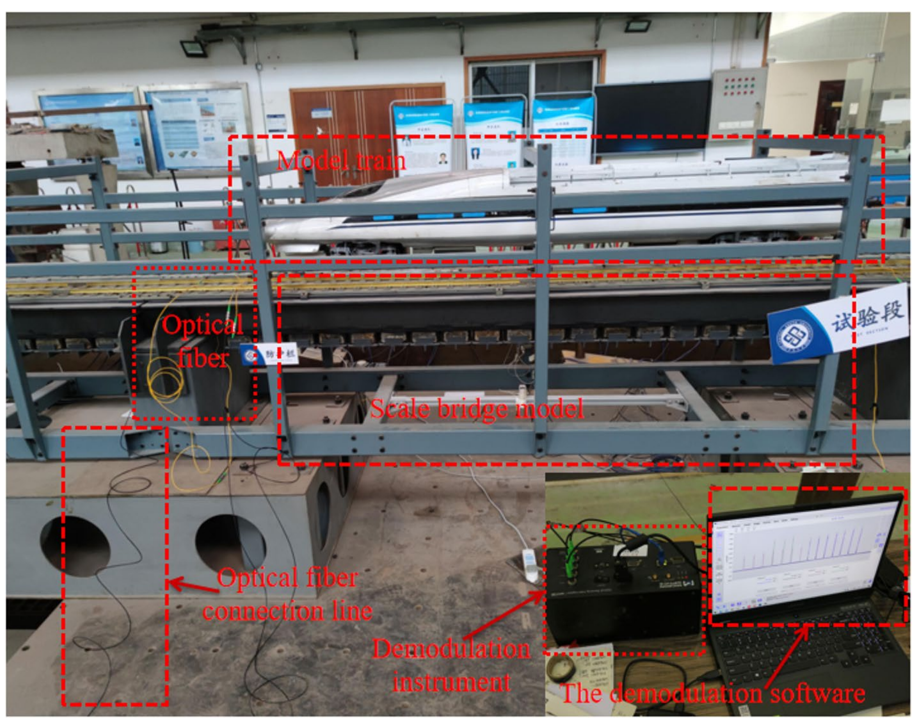

Fig. 7 Layout of the measuring equipment

Table 5 Experimental conditions

Vibration direction	Frequency	PGA	Train speed
Transverse	15 Hz	0.1 g	9 m/s
Transverse	15 Hz	0.1 g	13 m/s
Transverse	15 Hz	0.2 g	9 m/s
Transverse	15 Hz	0.2 g	13 m/s

The grating points on the rail, track slab, base plate and beam are numbered Ei, Fi, Gi and Hi (i = 1,2,3,4,5,6 and 7), respectively. Wherein, *i* mean the same coordinates in the train running direction.

The optical signal collected by the FBG sensors transmits to the demodulator through the optical fiber [8]. Subsequently, the demodulator inputs the demodulated strain data to a computer, which is displayed and stored in the computer through a computer program, shown in Fig. 7 [6].

Experimental conditions

In this research, the test conditions of the TRTS are listed in Table 5. In the experiments, the running speed of the model train is set to 9 m/s and 13 m/s (corresponding to the running speed of 100 km/h and 150 km/h in the prototype), respectively. Besides, a lateral 15 Hz sinusoidal wave with different PGAs is input as seismic excitation.

Results and discussion

Verification of the TBC model

Considering the similarity coefficients of the TRTS in Table 4, the strain time history of the bridge beam is measured in the experiment [5]. Wherein the train runs at a speed of 150 km/h and a 15 Hz sine wave with an amplitude of 0.1 g is input as the external excitation. Furthermore, the strain time history is converted to a PSD spectrogram using the fast Fourier transform, compared with a PSD spectrogram of the beam in the simulation results, shown in Fig. 8.

Compared with the experiment, the frequency components of the track structures and beam in the simulation results are close enough. Therefore, the TBC system established is feasible and accurate. Besides, it can be seen from Fig. 8 that the main vibration frequency of the beam corresponds to the sine wave frequency. Meanwhile, the track structure has lower frequency vibration than the sine wave frequency. This phenomenon is because the seismic action is transmitted from bottom to top, and the seismic vibration energy of the track structures is weakened after the beam consumes part of the vibration energy. In addition, there are different vibration frequency

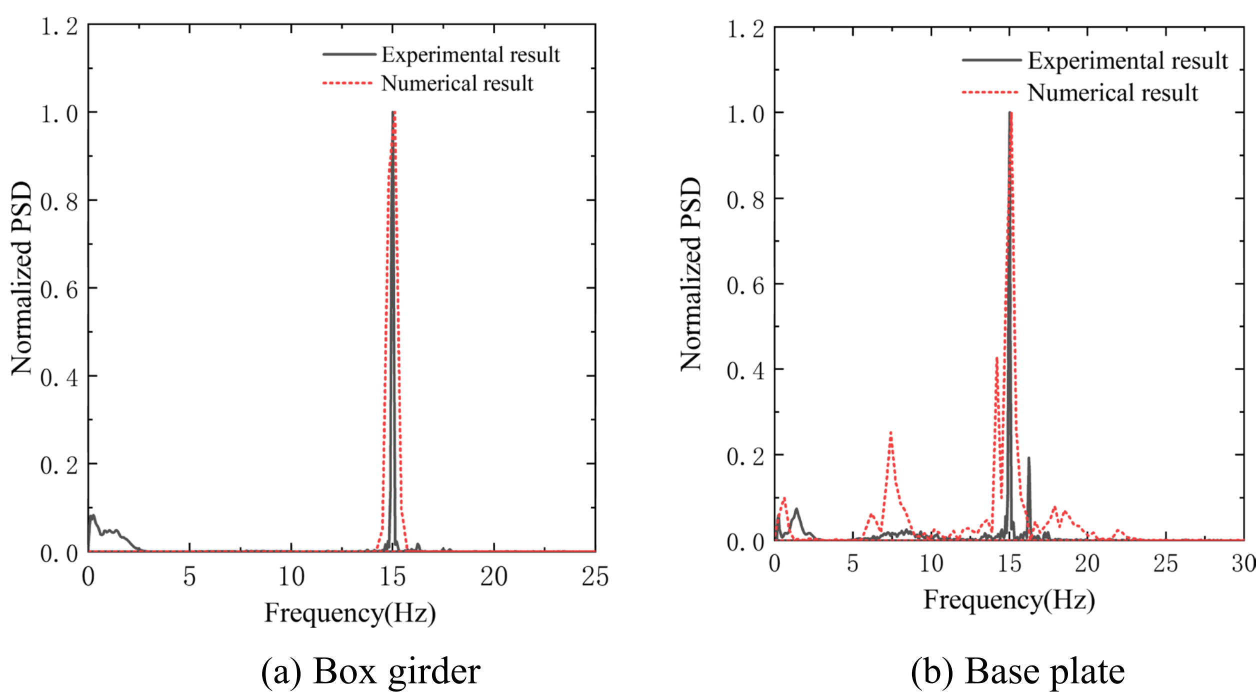

Fig. 8 Comparison of experimental and model frequency results

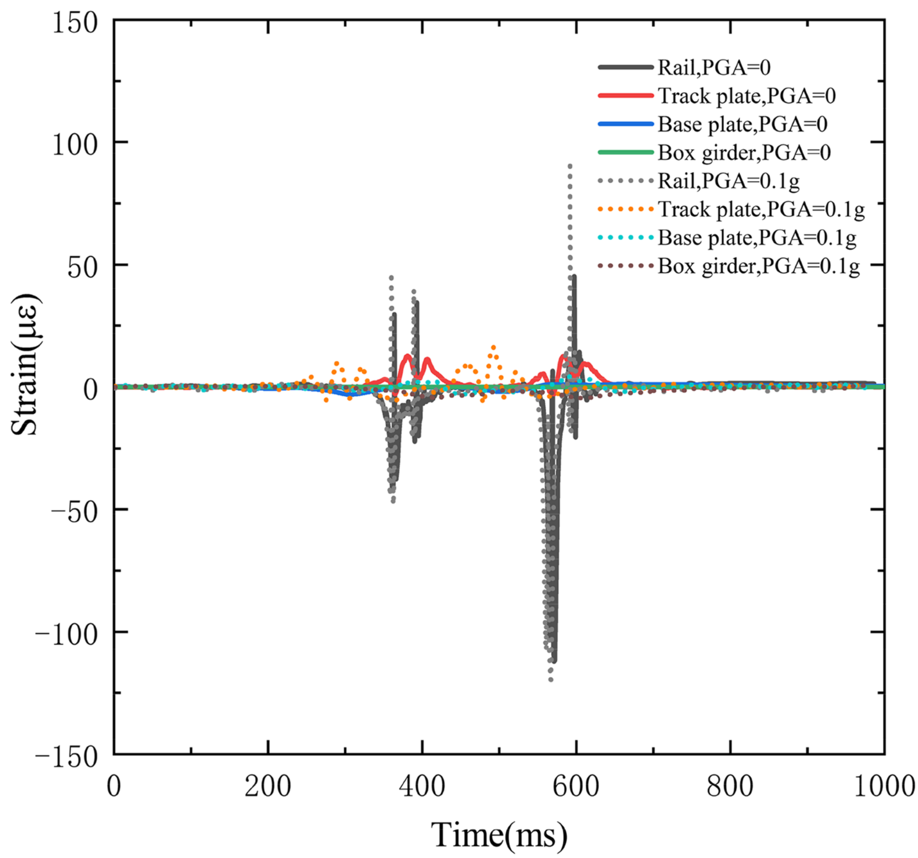

Fig. 9 Strain response of track structure and beam

Table 6 The maximum strain of the track structures and beam (unit:με)

Bridge members	Rail	Track slab	Base plate	Box girder
9 m/s, PGA = 0	112.12	12.77	3.03	2.90
13 m/s, PGA = 0	125.63	15.15	3.15	3.01
9 m/s, PGA = 0.1 g	119.66	16.30	4.31	3.41
13 m/s, PGA = 0.1 g	150.82	17.13	4.50	3.69
9 m/s, PGA = 0.2	125.37	18.31	4.88	4.03
13 m/s, PGA = 0.2	152.27	18.48	5.03	4.86

component differences between the train and the bridge structures. The track structure is also subject to the train load except for the sine wave frequency.

Experiment results analysis

Figure 9 shows the strain time history of the span-mid with and without the sinusoidal wave excitation when the train is running at 9 m/s speed. The maximum strain in Fig. 9 is −112.12με and −119.66με for the rail, 12.77με and 16.30με for the track slab, −3.03με and 4.31με for the base plate, −2.90με and −3.41με for the beam, respectively. In the TRTS, the strain response of the track structure decreases from top to bottom. The fastener resistance and the buffer effect of the CA mortar layer play an important role in reducing the strain of the track structures.

Table 6 lists the maximum strain of the track structures and beam under different test conditions. It can be concluded that the increase of train speed and PGA enhance the structural strain. Wherein the strain of the

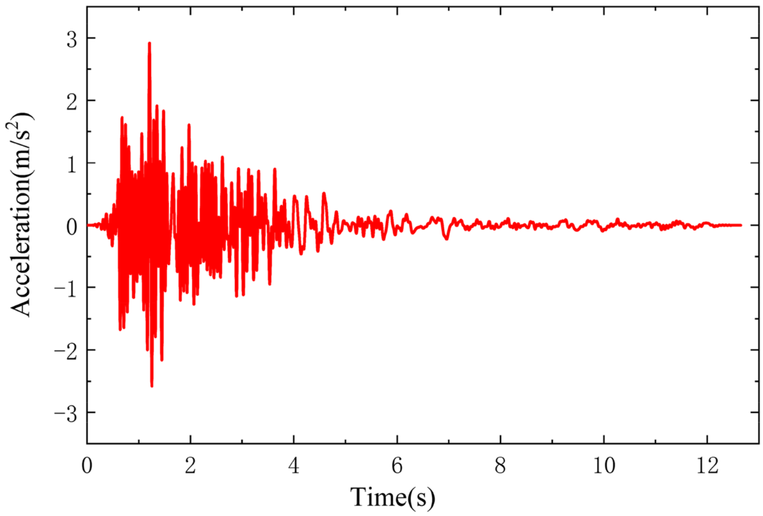

Fig. 10 Lateral acceleration time history of the input earthquake

track structures and beam decreases in turn, indicating that fasteners and CA mortar layer can reduce and isolate the earthquake.

Simulation results analysis

After verifying the accuracy of the TBC model, a ground motion (shown in Fig. 10) is input into the TBC system to calculate the three-dimensional acceleration of the track structure (rail, track plate, base plate) and beam under earthquake. The bridge site is located in the 8-degree fortification zone [38], and the seismic wave used in the article is randomly selected from the Pacific Earthquake Engineering Research Center earthquake database [2, 38]. Besides, the input seismic PGA is from 0.1 g to 0.4 g with an interval of 0.1 g, and the train speed is from 100 km/h to 300 km/h with an interval of 50 km/h. Figs. 11 and 12 shows the acceleration and displacement time history curves of the 7th mid-span when the train running speed is 100 km/h and the seismic PGA is 0.1 g, respectively.

The X, Y and Z directions stand for the longitudinal, transverse, and vertical directions. According to Fig. 11, it can be seen that the track structure and beam have the same tendency in acceleration time history curves in the X and Y directions. The track and beam are significantly affected by train load in the Z direction, and are hardly affected by earthquake, which is reflected in the sharp rise of acceleration time histories when the train passes through. The rail acceleration is greater than that of other structures, and the acceleration of each track structure decreases from the top to the bottom of the track structure. These phenomena are caused by the laterally applied earthquake. Therefore, the acceleration of the track structure and the beam is nearly consistent in the Y direction. In the Z direction, the fastener resistance weakens the force transferred to the lower structures, and the CA mortar layer acts as a buffer layer to further reduce the vibration of the base plate. That explains the acceleration decreases from top to bottom.

It can be seen in Fig. 12 that the displacement time history curves of rails, track plates, base plates and beams are consistent with the acceleration time history curves in X and Y directions. The displacement of the track structure is mainly caused by the train load. The displacement of the track plate, base plate and beam is consistent, and the rail displacement is greater than these three.

It can be seen from the three-dimensional time history curve that the Y direction is mainly affected by the earthquake, and the Z direction is mainly caused by train load in comparison. The dynamic response of rail is stronger than the other structures. In the seismic design for the HSR bridge structure, the lateral seismic performance should be emphasized, and the vertical response of the rail shall not be ignored.

The maximum displacement and acceleration of track structures and beam in the Y and Z directions under all test conditions are shown in Figs. 13 and 14. It can be observed that the maximum displacement will not increase with the uplift of train speed in the Y direction for the track structures and beam. Differently, the increase of PGA will magnify the maximum displacement of the track structures and beam.

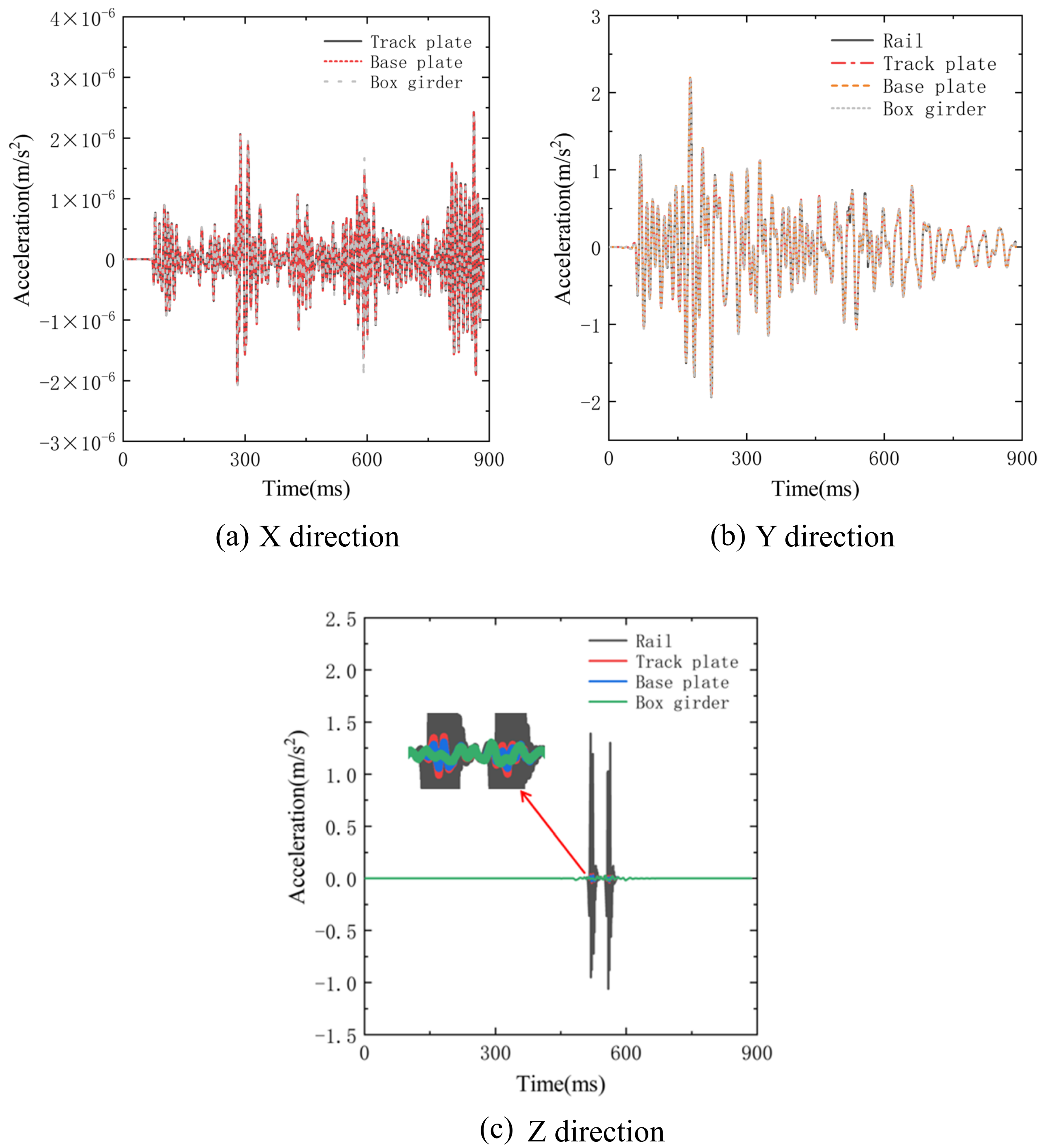

Fig. 11 Track structure and beam acceleration when V = 100 km/h, PGA = 0.1 g

In addition, the maximum rail displacement is always greater than the other track structures and beam, and the maximum displacement of the track slab, base plate and beam are always consistent. When the train runs at a lower speed, the maximum displacement of the track structures and beam slowly increases with the uplift of train speed. However, when the train speed exceeds 200 km/h, the maximum displacement

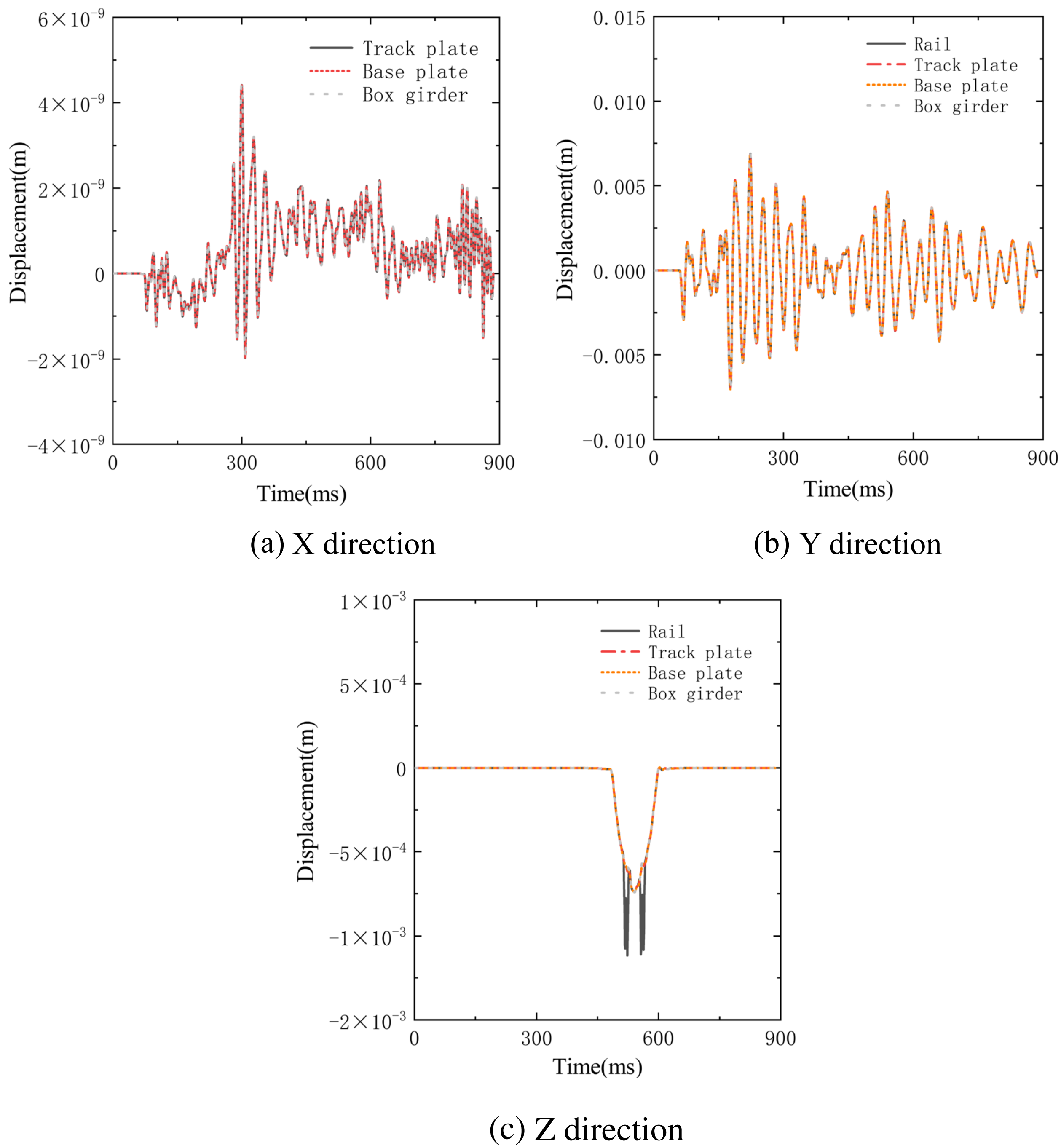

Fig. 12 Track structure and beam displacement when V = 100 km/h, PGA = 0.1 g

of track structures and beam gradually decreases with the uplift of train speed. Nevertheless, no matter in the Y or Z direction, the maximum displacement of the track structures and beam under the same running speed and PGA value is basically consistent.

The maximum acceleration of the track structures in the Y direction shows no correlation with the train speed, but it will increase with the increase of the PGA. In the Z direction, the maximum accelerations of the track structures and beam decrease in turn under the same train speed and PGA. Unlike those

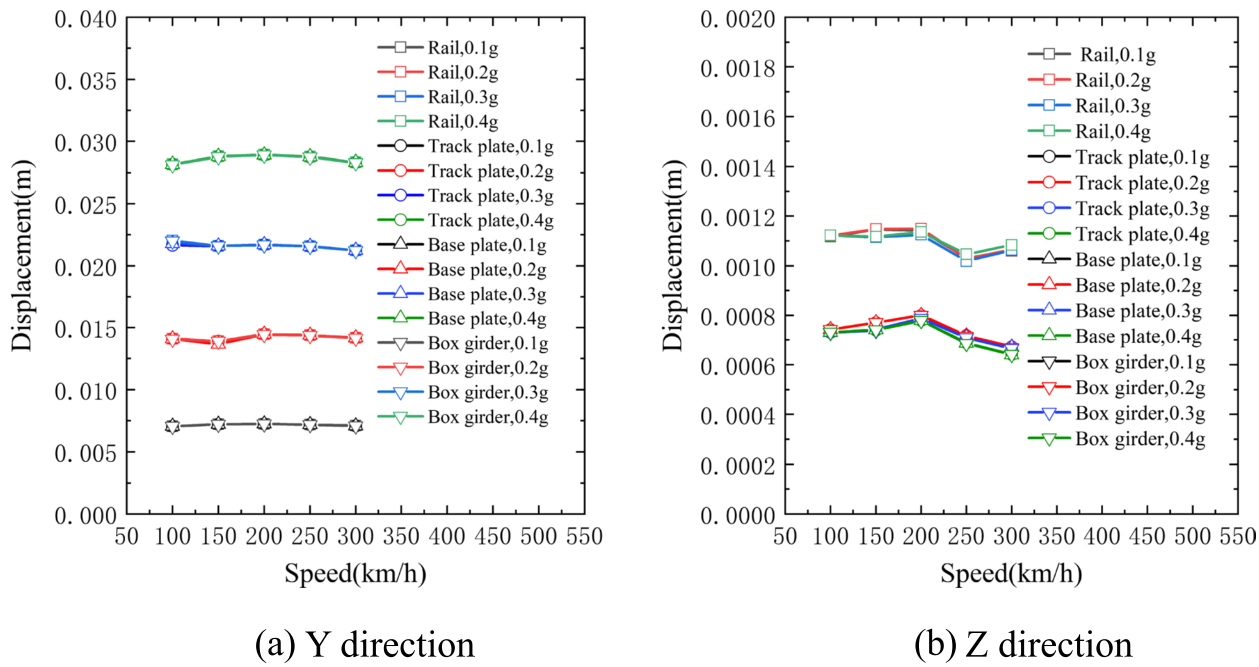

Fig. 13 Maximum displacement absolute values of rail, track plate, base plate and beam

in the Y direction, the maximum acceleration of the track structures and beam increases with the uplift of train speed, and it will not be affected by the change of PGA. The increasing rate of the maximum acceleration of the track structures and beam also increases with the uplift of train speed.

The dynamic response increases with the rise of PGA in the Y direction, and the dynamic response increases with the uplift of train speed. The conclusion mentioned in Section 4.3 is verified again that the track structures and beam are mainly affected by the earthquake in the Y direction, and are mainly affected by the moving train in the Z direction.

Conclusion

In this research, in order to study the three-dimensional dynamic response of the bridge track structure and beam under earthquake, a scaled bridge model is built to obtain the structural strain response through shaking table tests. Furthermore, a TBC simulation model is established, and it is verified by the experiment results. The influence of train speed and seismic effect on track structure and beam in three directions is calculated and analyzed, and some important conclusions are drawn as follows:

1. The train running will also affect the maximum strain of the bridge track structure during the earthquake. Besides, the strain response of the track structure caused by train load will decrease from top to bottom, and fasteners and CA mortar layer significantly reduce the transmitted vibration. The train speed and seismic intensity will enlarge the dynamic response of the track structure.
2. The dynamic response of the bridge beam is mainly caused by the earthquake, and the dynamic response of the track structure is caused by the train load and the earthquake. The shaking table test results verify the accuracy of the TBC system, which can be further used to study the dynamic behavior of the train and bridge under earthquake.
3. The dynamic responses (acceleration and displacement) of the rail, track slabs, base plates and beam are mainly subjected to the earthquake in the transverse direction. Besides, it is affected jointly by the moving train load and earthquake longitudinally, which has limited influence on the bridge. The vertical dynamic responses are excited by the train load, so it is necessary to strengthen the isolation effect of the rail. In addition, the maximum accelerations of the track slab, base plate and beam decrease in turn.

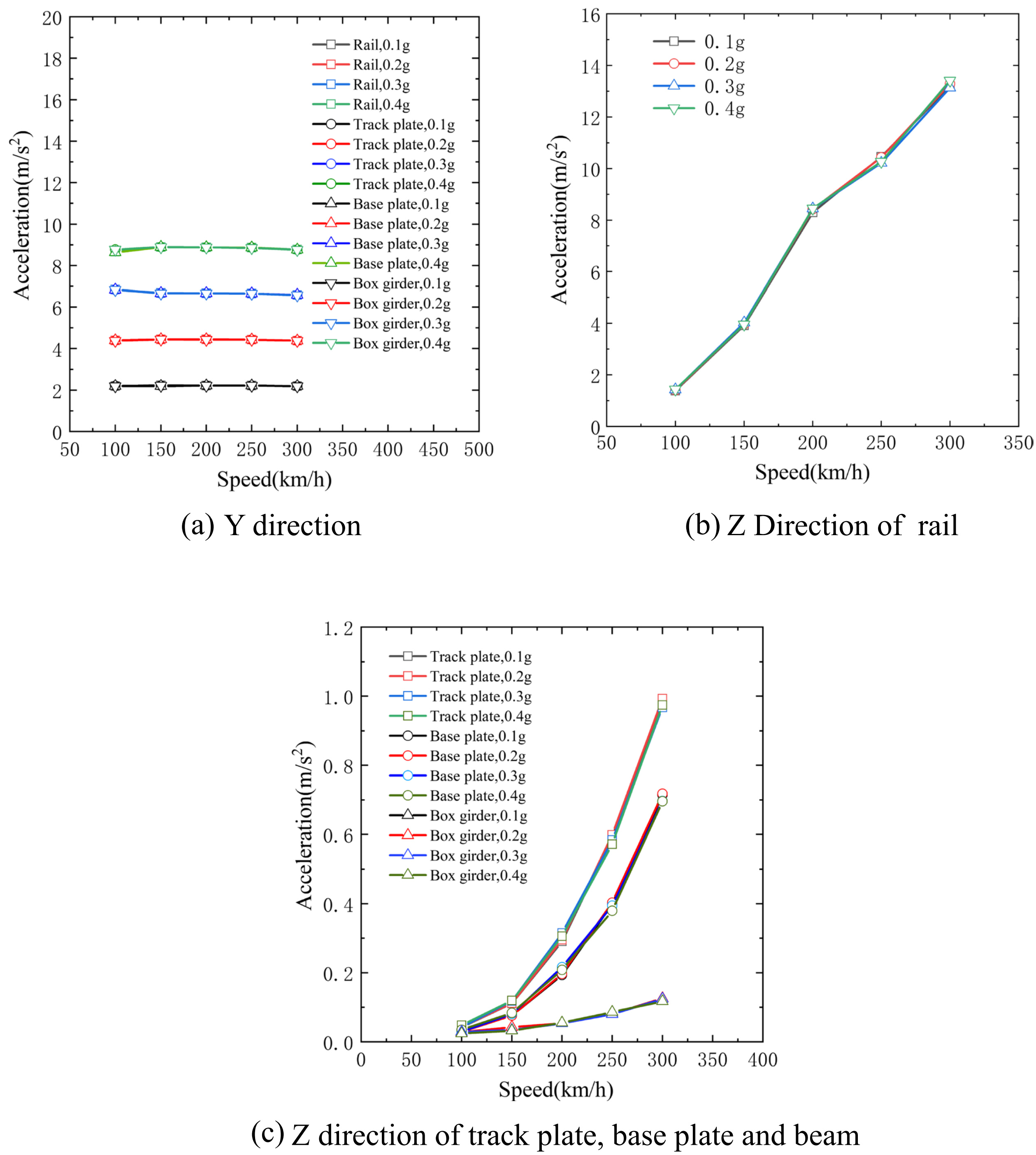

Fig. 14 Absolute value of the maximum acceleration of the rail, track slab, base plate and beam

4. The lateral dynamic responses of the rail, track slabs, base plates and beam will increase with the uplift of seismic PGA, but they are almost independent of the train speed. Besides, the maximum vertical displacement increases with the uplift of the train speed. The vertical accelerations of the rail, track slabs, base plates and beam increase with the uplift of the train speed. Wherein the increasing rate of the track slabs, base plates and beam rises with the growth of train speed.

Abbreviations

HSR	High-speed railway
FEM	Finite element method
TRTS	Train running test system
TBC	Train-bridge coupled
DOF	Degree of freedom
CRH2	China Railways High-speed 2
FBG	Fiber Bragg Grating
PSD	Power spectral density
PGA	Peak ground acceleration

Acknowledgements
The funding from Central South University and National Natural Science Foundation of China is greatly acknowledged.

Authors' contributions
X.B. Zhang: Modeling, Analysis, Writing - original draft. H. Wu: Conceptualization, Methodology, Modeling, Formal analysis, Writing - original draft, Review. H. Zhao: Conceptualization, Methodology, Review & Editing. P. Xiang: Conceptualization, Methodology, Review & Editing, Supervision, Funding Acquisition. All authors read and approved the final manuscript.

Funding
This research work was jointly supported by the National Natural Science Foundation of China (Grant No. 11972379), the key R&D program of Hunan Province (2020SK2060), and Hunan Science Fund for Distinguished Young Scholars (2021JJ10061).

Availability of data and materials
The analysis models used in the current study are available from the corresponding author on reasonable request.

Declarations

Ethics approval and consent to participate
Not applicable.

Consent for publication
Not applicable.

Competing interests
The authors declare that they have no known competing financial interests or personal relationships that could have appeared to influence the work reported in this paper.

Received: 11 December 2022 Revised: 19 January 2023 Accepted: 21 January 2023
Published online: 31 May 2023

References

1. Berrah MK, Kausel E (1993) A modal combination rule for spatially varying seismic motions. Earthq Eng Struct Dyn 22(9):791–800. https://doi.org/10.1002/eqe.4290220905
2. Center, P.E.E.R (2022) Ground motion database. Pacific Earthquake Engineering Research Center. https://ngawest2.berkeley.edu/site
3. Changqing L, Junping J, Lizhong J, Yang TY (2016) Theory and implementation of a two-step unconditionally stable explicit integration algorithm for vibration analysis of structures. Shock Vib 2016:1–8. https://doi.org/10.1155/2016/2831206
4. Chen LK, Jiang LZ, Liu P (2012) Seismic response analyses of high-speed railway bridge round-ended piers using global bridge model. Int J Mater Prod Technol 44(1–2):35–46. https://doi.org/10.1504/Ijmpt.2012.048190
5. Deng Y, Shi X (2022a) An accurate, reproducible and robust model to predict the rutting of asphalt pavement: neural networks coupled with particle swarm optimization. IEEE Trans Intell Transp Syst 23(11):22063–22072. https://doi.org/10.1109/TITS.2022.3149268
6. Deng Y, Shi X (2022b) Development of predictive models of asphalt pavement distresses in Idaho through gene expression programming. Neural Comput Applic 34(17):14913–14927. https://doi.org/10.1007/s00521-022-07305-2
7. Du XT, Xu YL, Xia H (2012) Dynamic interaction of bridge-train system under non-uniform seismic ground motion. Earthq Eng Struct Dyn 41(1):139–157. https://doi.org/10.1002/eqe.1122
8. Fan L, Shi X (2022) Techniques of corrosion monitoring of steel rebar in reinforced concrete structures: a review. Struct Health Monit 21(4):1879–1905. https://doi.org/10.1177/14759217211030911
9. Gao XJ, Duan PH, Qian H (2020) Dynamic response analysis of long-span continuous bridge considering the effect of train speeds and earthquakes. Int J Struct Stab Dyn 20(6):2040013. https://doi.org/10.1142/S0219455420400131
10. Gou H, Yang L, Mo Z, Guo W, Shi X, Bao Y (2019) Effect of long-term bridge deformations on safe operation of high-speed railway and vibration of vehicle-bridge coupled system. Int J Struct Stab Dyn 19(9). https://doi.org/10.1142/s0219455419501116
11. Gou HY, Liu C, Xie R, Bao Y, Zhao LX, Pu QH (2021) Running safety of high-speed train on deformed railway bridges with interlayer connection failure. Steel Compos Struct 39(3):261–274. https://doi.org/10.12989/scs.2021.39.3.261
12. Guo W, Wang Y, Zeng C, Wang T, Gu Q, Zhou HM, Zhou LY, Hou WQ (2021) Moving safety evaluation of high-speed train on post-earthquake bridge utilizing real-time hybrid simulation. J Earthq Eng. https://doi.org/10.1080/13632469.2021.1999869
13. He X, Nan Z, Weiwei G (2018) Dynamic interaction of train-bridge systems in high-speed railways. Springer, Berlin Heidelberg. https://doi.org/10.1007/978-3-662-54871-4
14. Hu P, Zhang F, Han Y, Zhou X, Xu G (2022) Dynamic responses of the rail vehicle-bridge coupling system considering the spanwise correlation functions in vehicle aerodynamic forces. Adv Struct Eng 25(6):1323–1338. https://doi.org/10.1177/13694332211064666
15. Jiang LZ, Feng YL, Zhou WB, He BB (2019a) Vibration characteristic analysis of high-speed railway simply supported beam bridge-track structure system. Steel Compos Struct 31(6):591–600. https://doi.org/10.12989/scs.2019.31.6.591
16. Jiang LZ, Liu X, Xiang P, Zhou WB (2019b) Train-bridge system dynamics analysis with uncertain parameters based on new point estimate method. Eng Struct 199. https://doi.org/10.1016/j.engstruct.2019.109454
17. Jin N, Yang YB, Dimitrakopoulos EG, Paraskeva TS, Katafygiotis LS (2021) Application of short-time stochastic subspace identification to estimate bridge frequencies from a traversing vehicle. Eng Struct 230. https://doi.org/10.1016/j.engstruct.2020.111688
18. Johnson KL (1985) Contact mechanics. Cambridge University Press. https://doi.org/10.1017/CBO9781139171731
19. Kalker JJ (2013) Three-dimensional elastic bodies in rolling contact. Springer Science & Business Media, Dordrecht. https://doi.org/10.1007/978-94-015-7889-9
20. Kang CJ, Schneider S, Wenner M, Marx S (2020) Experimental investigation on rail fatigue resistance of track/bridge interaction. Eng Struct 216:110747. https://doi.org/10.1016/j.engstruct.2020.110747
21. Kang CJ, Schneider S, Wenner M, Marx S (2021) Experimental investigation on the fatigue behaviour of rails in the transverse direction. Constr Build Mater 272:121666. https://doi.org/10.1016/j.conbuildmat.2020.121666
22. Lai ZP, Jiang LZ, Liu X, Zhang YT, Zhou WB (2021) Analytical investigation on the geometry of longitudinal continuous track in high-speed rail corresponding to lateral bridge deformation. Constr Build Mater 268:121064. https://doi.org/10.1016/j.conbuildmat.2020.121064
23. Li HY, Yu ZW, Mao JF, Spencer BF (2021) Effect of seismic isolation on random seismic response of high-speed railway bridge based on probability density evolution method. Structures 29:1032–1046. https://doi.org/10.1016/j.istruc.2020.11.070
24. Ling L, Xiao XB, Jin XS (2012) Study on derailment mechanism and safety operation area of high-speed trains under earthquake. J Comput Nonlinear Dyn 7(4):041001. https://doi.org/10.1115/1.4006727
25. Liu X, Jiang L-Z, Xiang P, Lai Z-P, Feng Y-L, Cao S-S (2021) Dynamic response limit of high-speed railway bridge under earthquake considering running safety performance of train. J Cent South Univ 28(3):968–980. https://doi.org/10.1007/s11771-021-4657-2

26. Liu X, Jiang LZ, Lai ZP, Xiang P, Chen YJ (2020) Sensitivity and dynamic analysis of train-bridge coupled system with multiple random factors. Eng Struct 221. https://doi.org/10.1016/j.engstruct.2020.111083
27. Nishimura K, Terumichi Y, Morimura T, Adachi M, Morishita Y, Miwa M (2015) Using full scale experiments to verify a simulation used to analyze the safety of rail vehicles during large earthquakes. J Comput Nonlinear Dyn 10(3):031013. https://doi.org/10.1115/1.4027756
28. Odikamnoro I, Badal PS, Burton H, Tesfamariam S (2022) Seismic collapse risk of rc-timber hybrid building with different energy dissipation connections considering nbcc 2020 hazard. J Infrastruct Preserv Resil 3(1):14. https://doi.org/10.1186/s43065-022-00061-6
29. Song H-X, Ke L-L, Su J, Yang J, Kitipornchai S, Wang Y-S (2020) Surface effect on the contact problem of a piezoelectric half-plane. Int J Solids Struct 185-186:380–393. https://doi.org/10.1016/j.ijsolstr.2019.07.024
30. Su M, Dai GL, Peng H (2020) Bond-slip constitutive model of concrete to cement-asphalt mortar interface for slab track structure. Struct Eng Mech 74(5):589–600. https://doi.org/10.12989/sem.2020.74.5.589
31. Toyooka A, Ikeda M, Yanagawa H, Kataoka H, Iemura H, Murata K (2005) Effects of track structure on seismic behavior of isolation system bridges. Q Rep RTRI 46(4):238–243. https://doi.org/10.2219/rtriqr.46.238
32. Xia H, Han Y, Zhang N, Guo WW (2006) Dynamic analysis of train-bridge system subjected to non-uniform seismic excitations. Earthq Eng Struct Dyn 35(12):1563–1579. https://doi.org/10.1002/eqe.594
33. Xiang P, Ma HK, Zhao H, Jiang LZ, Xu SP, Liu X (2023) Safety analysis of train-track-bridge coupled braking system under earthquake. Structures 53(1):1519–1529. https://doi.org/10.1016/j.istruc.2023.04.086
34. Xu L, Zhai WM (2019) A three-dimensional model for train-track-bridge dynamic interactions with hypothesis of wheel-rail rigid contact. Mech Syst Signal Process 132:471–489. https://doi.org/10.1016/j.ymssp.2019.04.025
35. Yang YB, Wang BQ, Wang ZL, Shi K, Xu H, Zhang B, Wu YT (2020a) Bridge surface roughness identified from the displacement influence lines of the contact points by two connected vehicles. Int J Struct Stab Dyn 20(14). https://doi.org/10.1142/S0219455420430038
36. Yang YB, Xiong F, Wang ZL, Xu H (2020b) Extraction of bridge frequencies inclusive of the higher modes by the esmd using the contact-point response. Int J Struct Stab Dyn 20(4). https://doi.org/10.1142/S0219455420500455
37. Yu J, Jiang L, Zhou W, Liu X, Nie L, Zhang Y, Feng Y, Cao S (2021a) Running test on high-speed railway track-simply supported girder bridge systems under seismic action. Bull Earthq Eng 19(9):3779–3802. https://doi.org/10.1007/s10518-021-01125-w
38. Yu J, Jiang L, Zhou W, Lu J, Zhong T, Peng K (2021b) Study on the influence of trains on the seismic response of high-speed railway structure under lateral uncertain earthquakes. Bull Earthq Eng 19(7):2971–2992. https://doi.org/10.1007/s10518-021-01085-1
39. Yu J, Jiang LZ, Zhou WB, Liu X, Lai ZP (2022) Seismic-induced geometric irregularity of rail alignment under transverse random earthquake. J Earthq Eng 1-22. https://doi.org/10.1080/13632469.2022.2030437
40. Zhai W (2020) Vehicle–track coupled dynamics: theory and applications springer nature. https://doi.org/10.1007/978-981-32-9283-3
41. Zhang YT, Jiang LZ, Zhou WB, Feng YL, Tan ZH, Chai XL (2020) Study of bridge-subgrade longitudinal constraint range for high-speed railway simply-supported beam bridge with crtsii ballastless track under earthquake excitation. Constr Build Mater 241:118026. https://doi.org/10.1016/j.conbuildmat.2020.118026
42. Zhang Z, Zhang Y, Lin J, Zhao Y, Howson WP, Williams FW (2011) Random vibration of a train traversing a bridge subjected to traveling seismic waves. Eng Struct 33(12):3546–3558. https://doi.org/10.1016/j.engstruct.2011.07.018
43. Zhao H, Wei B, Jiang L, Xiang P (2022) Seismic running safety assessment for stochastic vibration of train–bridge coupled system. Arch Civil Mech Eng 22(4):180. https://doi.org/10.1007/s43452-022-00451-3
44. Zhao H, Wei B, Jiang LZ, Xiang P, Zhang XB, Ma HK et al (2023) A velocity-related running safety assessment index in seismic design for railway bridge. Mech Syst Signal Process 198(1):110305. https://doi.org/10.1016/j.ymssp.2023.110305

Publisher's Note

Springer Nature remains neutral with regard to jurisdictional claims in published maps and institutional affiliations.